

## Additive Manufacturing of High-Entropy Alloys – A Review

Wenyuan Cui\*, Xinchang Zhang\*, Frank Liou\*

\*Department of Mechanical and Aerospace Engineering, Missouri University of Science and  
Technology, Rolla, MO, 65409

### Abstract

High-entropy alloys have attracted increasingly interest due to their unique compositions, microstructures and mechanical properties. Additive manufacturing has been recognized as a promising technology to fabricate the high-entropy alloys in the recent years. The purpose of this paper is to review the current research progress in high-entropy alloys by additive manufacturing process. It will first highlight the important theory of the high-entropy alloys. The next aspect is to summarize current additive manufacturing methods applied for the high entropy alloys. At last, the correlation between the microstructures and the mechanical properties of the high-entropy alloys will be examined and discussed.

**Keywords:** Additive Manufacturing; High-Entropy Alloys; Microstructures; Mechanical Properties

### Introduction

High-entropy alloys (HEAs) were first proposed by Yeh et al. and have attracted increasingly attention from the researchers and scientists [1]–[10]. The conventional metallic alloys usually are choosing one principal element with small amounts of other elements added to improve the properties. By contrast, HEAs are defined as alloys that have at least five principal elements and the concentration of each element is between 5 at. % to 35 at.%. Yeh summarized the core effects for HEAs: high-entropy effect, sluggish diffusion, severe lattice distortion and cocktail effects [1]–[3]. The high-entropy effect implies that the high mixing entropy of the elements leads to the formation of single-phase solid solution with simple crystal structures like face-center cubic (fcc) or body-center cubic (bcc) rather than intermetallic. In HEAs, the properties can be influenced by adjusting the composition change and this is called cocktail effect. It has been a challenge for the researchers to investigate the fundamental of HEAs due to the lack of the thermodynamic database and phase diagrams. Current approaches and rules to predict the phases in HEAs are based on the empirical equations like Gibbs energy, mixing entropy and mixing enthalpy [9][11]. Zhang and Yang proposed the parameters of  $\Omega$  and atomic size  $\delta$  as a starting point to predict the formation of solid-solution phases [6], [7]. Valence electron concentration (VEC) is another criterion to decide the bcc or fcc crystal structure in HEAs [12]. These parameters have been applied in some alloys systems.

The microstructures and mechanical properties of HEAs have been reported indicating their high strength, wear resistance, ductility and corrosion resistance [5], [6], [9], [13]–[15]. Most of the work utilized casting or arc melting to produce HEAs. However, it is not easy to overcome the inherent complexity and high degree of controls by the traditional manufacturing methods [16],

[17]. Moreover, it is unlikely to design the industrially suitable route to mass produce HEAs. As a result, additive manufacturing (AM) with a higher level of local process and rapid solidification rate will be a promising way to produce HEAs as engineering materials [18], [19]. Wu et al. successfully synthesized FeCoCrAlCuNi<sub>x</sub>, FeCoCrAlNiTi<sub>x</sub>, FeCoCrAlNi HEAs coatings free of cracks and pores by laser surface alloying [20]–[22]. Selective laser sintering (SLM) was chosen to produce FeCoCrNi HEA and it showed high strength and ductility comparable to the stainless steel [16]. AlCoCrFeNi HEA produced by selective electron beam melting (SEBM) demonstrated six times higher fracture strength than that of a conventional engineering material [17], [23].

This work aims to provide a thorough literature review on the powder feed and powder bed laser additive manufacturing process of the common HEA parts. It will first introduce the general concept of HEAs design and unique characteristics of powder feed and powder bed laser additive manufacturing. Furthermore, the bulk of the work will focus on the evaluation of microstructures, mechanical properties together with the corrosion resistance of HEAs.

### Theory of High-Entropy Alloys

The prediction and the stability of the solid solutions have been a topic of significant importance in current HEAs research. Thermodynamics parameters like Gibbs energy, entropy and enthalpy among the phase competition in HEAs were delicately discussed [8], [24]. For the random solid-solution system of N component, the configuration entropy can be expressed in **Eq. (1)**. Since HEAs possess more than five principal components, it increases the extent of confusion in the system and mixing entropy.

A common approach is the utilization of Hume-Rothery rule, which the atomic size ( $\delta$ ) and the mixing enthalpy ( $\Delta H_{mix}$ ) are the two domain factors to form substitutional solid solutions. Zhang et al. proposed the parameter  $\delta$  to study the relationship between the phase stability and the difference in atomic size between the N-element compositions **Eqs. (2), (3)** [5]–[7].

$$\Delta S_{mix} = -R \sum_{i=1}^n C_i \ln C_i \quad (1)$$

$$\Delta H_{mix} = 4 \sum_{i=1, i \neq j}^n \Delta H_{ij}^{mix} C_i C_j \quad (2)$$

$$\delta = 100 \sqrt{\sum_{i=1}^n C_i (1 - r_i / \sum_{i=1}^n c_i r_i)^2} \quad (3)$$

where  $\Delta H_{mix}$  are the mixing enthalpy between the A element and B element,  $c_i$  is the molar concentration of the  $i$ th component and  $r_i$  is the atomic radius of the  $i$ th component. It indicates that the solid-solution formation requires  $\delta \leq 6.6\%$ .

Yang et al. established another parameter  $\Omega$  which defines the combined effects between  $\Delta S_{mix}$  and  $\Delta H_{mix}$  used to predict the solid-solution phase formation in HEA [7], [9].

$$\Omega = \frac{T_m \Delta S_{mix}}{|\Delta H_{mix}|} \quad (4)$$

$$T_m = \sum_{i=1}^n c_i (T_m)_i \quad (5)$$

where  $T_m$  is the average melting temperatures of the N-components in the alloy system. By analyzing the equations above, Yang pointed out that  $\Omega=1$  is a critical value to form the solid solution. For  $\Omega>1$ , the contribution of  $\Delta H_{mix}$  is less than that of  $T_m\Delta S_{mix}$  and the multi-component system consists of the solid solutions.

Guo et al. studied the stability of face-center cubic(fcc) and body-center cubic(bcc) solid solutions are determined by valence electron concentration (VEC) [12]. A higher valence electron concentration ( $VEC\geq 8$ ) favors the fcc solid solutions and bcc solid solution is stabilized at a lower value ( $VEC<6.87$ ). The VEC values of HEAs are expressed in Eq. (6).

$$VEC = \sum_{i=1}^n C_i(VEC)_i \quad (6)$$

where  $c_i$  is the molar concentration for the  $i$ th component,  $(VEC)_i$  is the valence electron concentration for the individual  $i$ th composition.

**Table 1** illustrates the alloy composition, the calculated values of  $\delta$ , VEC,  $\Omega$  and crystal structures reported by additive manufacturing. It can be seen that the formation of fcc or bcc solid solution is in good agreement with the calculated parameters for most of the cases. However, the crystal structure in a few alloys does not coincide with the parameter  $\delta$ . For example, FeCoCrAlNiTi<sub>1.5</sub> and FeCoCrAlNiTi<sub>2.0</sub>, the metastable phase Ti<sub>2</sub>Ni was reported along with fcc and bcc structures. This phenomenon could be mainly attributed to the improved solubility and a uniform compositional distribution in the rapid solidified laser coating. Moreover, it is pointed out that the rapid solidification reduces the solid-liquid surface energy of the metastable phases and stimulate the formation of the metastable phases in the alloy systems.

**Table 1 HEA crystal structures and thermal parameters reported by AM**

Alloy	$\delta$	VEC	$\Omega$	Crystal Structure	Ref.
FeCoCrAlNiTi <sub>0.5</sub>	6.19	6.92	–	fcc, bcc	[20]
FeCoCrAlNiTi <sub>1.0</sub>	6.6	6.68	–	fcc, bcc	[20]
FeCoCrAlNiTi <sub>1.5</sub>	6.83	6.47	–	fcc, bcc, Ti <sub>2</sub> Ni	[20]
FeCoCrAlNiTi <sub>2.0</sub>	6.94	6.29	–	fcc, bcc, Ti <sub>2</sub> Ni	[20]
AlFeCoCrNi	5.02	7.3	–	bcc	[25]
CoCrAlNiFe	5.438	7.2	–	bcc	[22]
NiCrCoTiVAl	6.74	5.02	–	bcc, $\alpha$ -Ti	[19]
AlCrFeNiCoCu	6	7.14	–	bcc, fcc	[8]
FeCoCrAlCuNi <sub>0.5</sub>	5.04	7.64	–	fcc, bcc	[21]
FeCoCrAlCuNi <sub>1.0</sub>	4.98	7.85	–	fcc, bcc	[21]
FeCoCrAlCuNi <sub>1.5</sub>	4.52	8.01	–	fcc	[21]
FeCoCrAlCuMo <sub>0.5</sub>	4.998	7.28	15.334	fcc, bcc, Fe <sub>2</sub> Mo	[26]
FeCoCrAlCuSi <sub>0.5</sub>	6.495	7.09	1.995	fcc, bcc	[26]
FeCoCrAlCuTi <sub>0.5</sub>	5.807	7.1	2.959	fcc, bcc, Fe <sub>2</sub> Ti	[26]

## Additive Manufacturing Methods

Most metallic powder additive manufacturing methods can be classified into three categories, (1) powder feed, (2) powder bed fusion and (3) wire feed process [23]. Most commonly used methods in HEAs are powder feed and powder bed fusion methods. A set up of direct metal deposition (DMD) with coaxial powder feeder is shown in **Figure 1**. During the process, a concentrated laser beam melts the synchronously fed powders and a thin layer of the substrate. The metallic powders undergo a rapid melting and cooling process. Meanwhile, a metallurgical bonding can be formed between the substrate and the powders.  $\text{Al}_x\text{FeCoCrNi}_x$  ( $x=0.3,1$ ) HEAs were fabricated by DMD [27]. Similar method of laser cladding is also applied in FeCoCrAlCu [21],  $\text{Al}_x\text{FeCoNiCuCr}$  [28]. Kuncce used the direct laser-engineered net shaping (LENS) for HEA as a hydrogen storage material [29].

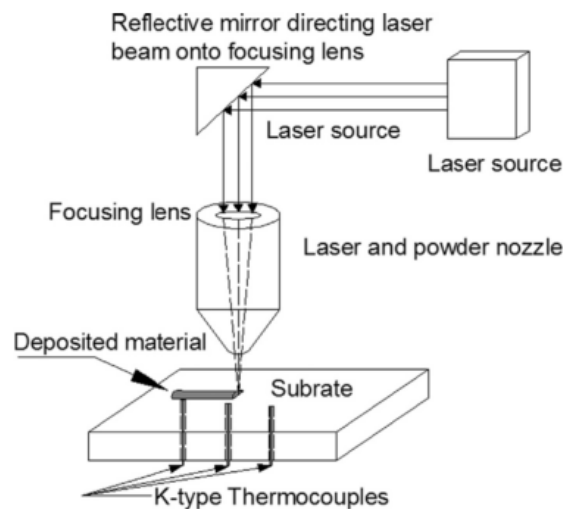


**Figure 1 Schematic diagram of direct metal deposition (DMD) process setup[30]**

For the laser-based additive manufacturing methods, the precursor metallic powders are melted by high energy laser or electron beam in a layer by layer manner[16], [31], [32]. A schematic selective laser melting (SLM) layout is present in **Figure 2**. The geometrically complex components with high dimension precision can be obtained by the SLM process without subsequent process. The inert Argon or Nitrogen is usually used as the atmosphere environment. Fujieda first reported the feasibility of this method used for AlCoCrFeNi HEA, which facilitated a high level of local process control and generated rapid solidification rates [17]. It showed the ductility and fracture strength were remarkably improved compared to the conventional methods. It was further explained the preheating process led to low residual stress and significantly affected the microstructures and mechanical properties[23], [33], [34].

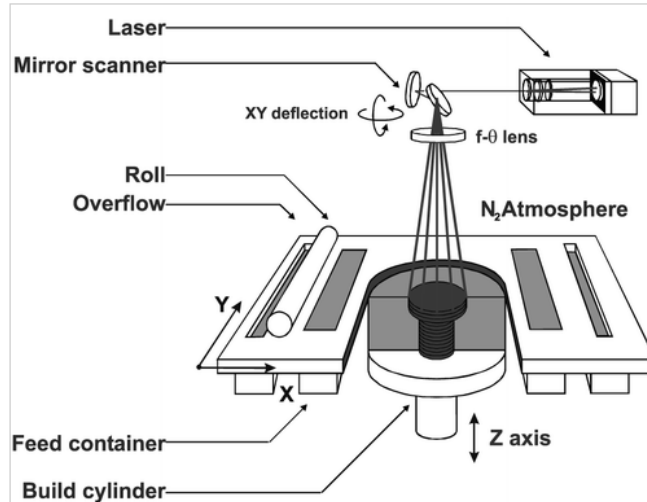


Figure 2 A typical selective laser melting (SLM) machine layout [31]

### Microstructure Characterization

Microstructures and mechanical properties of HEAs have been frequently investigated. As the metallic powders characteristics have critical an impact on the mechanical properties, some amount of studies have been conducted in this area. The pure elemental powders of Fe, Co, Ni, Cr and Cu (99.7% wt.% minimum) were mechanically mixed together and the particle sizes were about 50-120  $\mu\text{m}$  [31] Additives of Si and Mo were added into the FeCoNiCrCu powders as master alloys in order to avoid the different melting points and densities of nonmetallic elements. The morphology of the AlCoCrFeNi powders used for the HEA is in **Figure 3**. It was observed that the powder particles were spherical or nearly spherical with relatively smooth surface. But a few aggregates of the powder particles were formed due to the turbulent flow in the atomization chamber and the collision of the solidifying droplets [29].

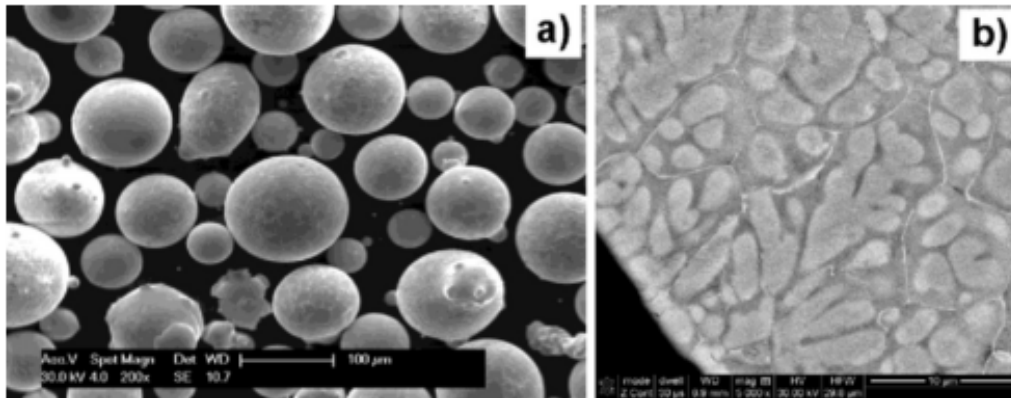
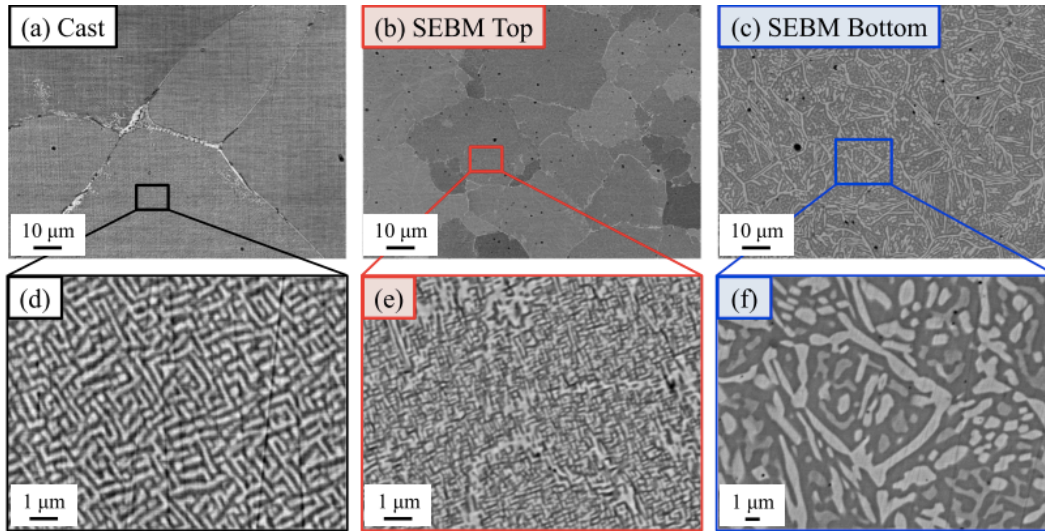


Figure 3 Morphology (a), SEM/BSE micrographs (b) of the AlCoCrFeNi powder particles[29]

**Figure 4** shows the SEM/BSE images of the AlCoCrFeNi HEAs cast and SEBM specimens. The images of the SEBM specimens were obtained at the cross-section perpendicular to the build direction. It is seen the cast specimens have much coarser grain sizes than the SEBM

counterparts (**Figure 4 a-c**). The SEBM specimens present the equiaxed grains, but the more coarsening of the modulated structure was seen at the bottom of the part.



**Figure 4** SEM images of the (a) cast, the SEBM (b) top and (c) bottom of AlCoCrFeNi HEA [23]

### Mechanical Properties

Mechanical properties of HEAs have been studied from the aspects of hardness, tensile and yield strength testing. The studies indicate that the mechanical properties of additive manufactured HEAs are comparable or better than the conventional alloys [24], [35]–[37]. Moreover, the process parameters, alloying element and post-treatment may cause remarkable effect on the mechanical properties.

Vickers hardness testing has been widely used in mechanical property characterization of HEAs. Vickers hardness of the most common HEAs are compared with the conventional Ni, Al and Fe and Ti based alloys in **Figure 5**. The hardness varies in one alloy system. For instance, the  $Al_xFeCoNiCuCr$  system, the hardness varies from 390HV to 687HV depending on the contents of Al. The hardness of several types of HEAs like AlCoCrFeCu, AlCrFeCoCuTiNi and AlCoCrFeNiTi are generally higher than the conventional alloys.

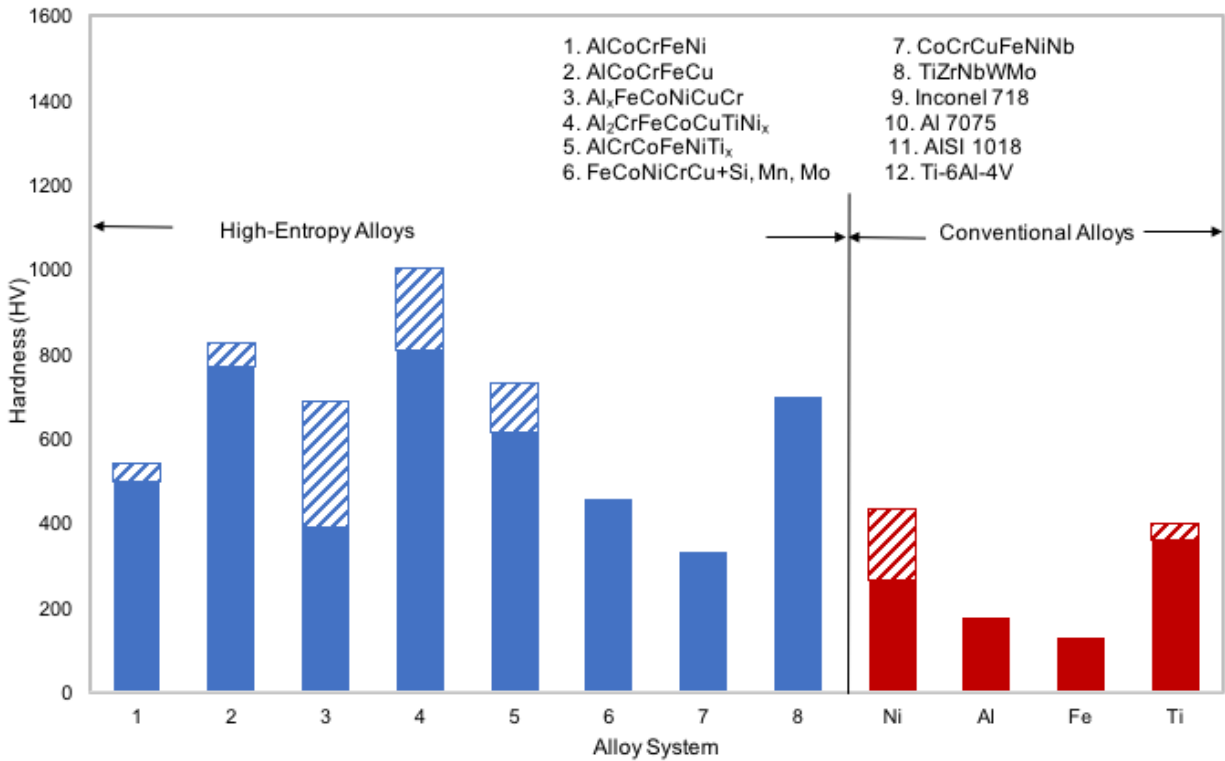


**Figure 5 Hardness of most common HEAs compared with the conventional alloys using the data from [9], [20], [22], [29], [38]–[44]**

The selection of alloys system is critical in determining the hardness of HEAs. The hardness has the trend of increase with the Ni content in **Figure 6**. Since more bcc crystal structure with higher microhardness formed within the alloy system, it enhances the corresponding microhardness of the HEA [40]. The addition of Al promotes the transition from fcc to bcc crystal structure in Al<sub>x</sub>FeCoNiCuCr system reported [28]. As the bcc is considered to be higher in microhardness than fcc structure, it shows a sharp increase when the X increases from 1.0 to 1.5. However, the addition of Al also increases the cracks. It indicates that the optimal X lies between 1.5 and 1.8 for a better balance of the microhardness and cracks.

Process parameters have significant effect on the hardness. It was found the average hardness of laser-produced AlCoCrCrNi samples were approximately 13% higher than the as-cast state [29]. This is due to the grain refinement of the LENS-produced samples. It also found that the microhardness increases with the cooling rate during the laser process. Zhang discussed that the rapid solidification during the laser process could suppress the grain growth and hence increase the amount of grain boundaries and form the grain boundary strengthening [39].

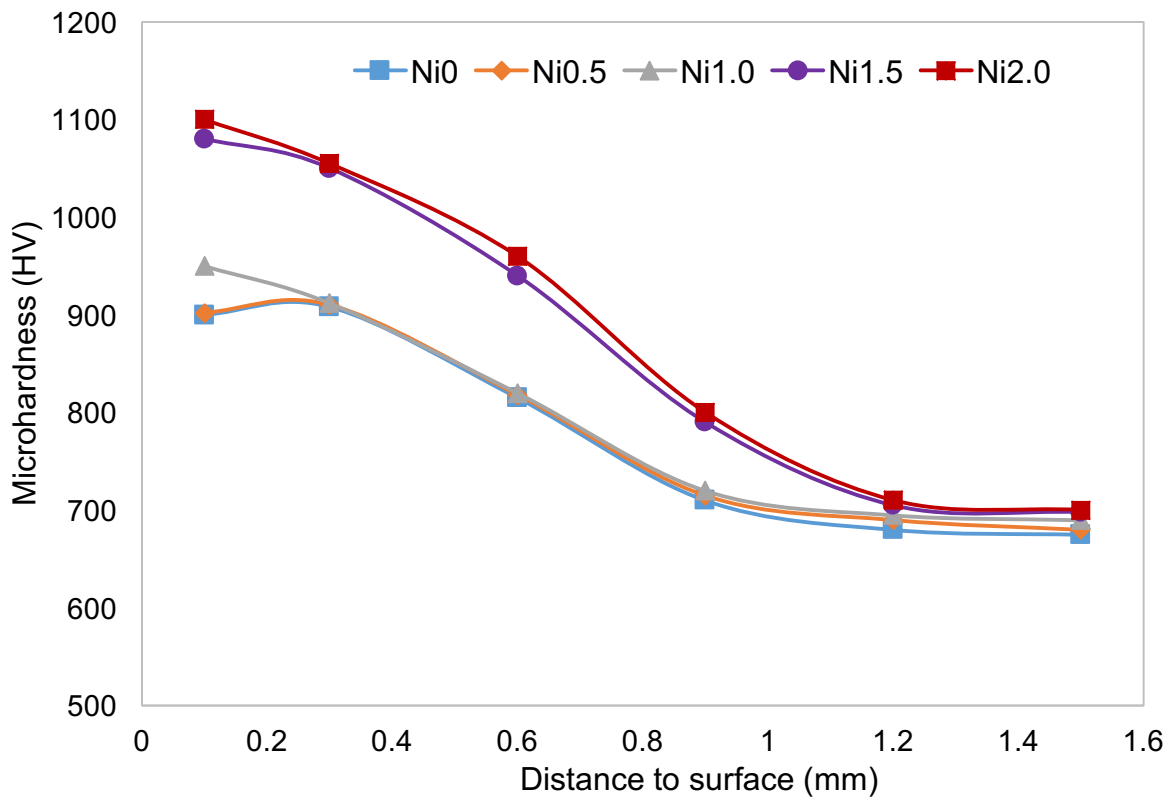


**Figure 6 Microhardness of Al<sub>2</sub>CrFeCoCuTiNix high-entropy alloys using the data from [40]**

Compressive tests are also applied to evaluate the mechanical properties of laser-produced HEAs in **Table 2**. It reported the overall compressive properties of AlCoCrFeNi specimens by SEBM were superior to those casting specimens [17]. The enhanced plasticity of SEBM specimens could be ascribed to the finer microstructure and existence of fcc phases, which had higher atomic packing factor and closer packed slip planes. Post heat treatment was conducted on the DML fabricated AlCoCrFeNi samples by Wang [45]. The softer fcc phase resulted in reduced yield strength with enhanced ductility and this was proved in their fractographic analysis.

**Table 2 Compressive properties of HEAs at room temperature**

Alloy	$\sigma_y$ (Gpa)	$\sigma_{max}$ (GPa)	$\epsilon_p$ (%)	Process	Ref.
AlCoCrFeNi	1.31	2.6	16.8	DML, 600°C/168h HT	[45]
	1.17	2.94	21.6	DML, 800°C/168h HT	[45]
	1.07	2.83	24.9	DML, 1000°C/168h HT	[45]
	1.13	3.02	24.2	DML, 1200°C/168h HT	[45]
AlCoCrFeNi	1.308±0.077	1.425±0.1275	5.6±1.9	Casting	[17]
	1.015±0.053	1.668±0.0715	26.4±6.7	<sup>1</sup> SEBM (0°)	[17]
	0.944±0.055	1.447±0.1358	14.5±5.3	<sup>2</sup> SEBM (90°)	[17]

<sup>1</sup> parallel to laser build direction, <sup>2</sup> perpendicular to laser build direction.

## Corrosion Resistance

The corrosion features of HEAs is determined by the interaction between the environment and materials [20], [46]–[48]. The common service environments include the salt water or acid. The corrosion-resistance of HEAs are usually affected by the alloying element, phase change, phase segregation. Some recent working concerning on corrosion-resistance of HEAs will be discussed here.

Wu et al. investigated the effect of Ni content in the alloy of FeCoCrAlCuNi<sub>x</sub> and Al<sub>2</sub>CrFeCoCuTiNi<sub>x</sub> coatings by laser cladding [20], [40]. SEM results showed the coating structure was consisted of heat-affected, bounding and cladding zones. Simple microstructure of fcc and bcc phases with columnar crystals were observed, which decreased the ingredient segregation. The corrosion current reduced 1 magnitude compared to Q235 carbon steel. Al<sub>2</sub>CrFeCoCuTiNi<sub>1.0</sub> exhibited the best resistance to corrosion in the tests. However, with the increase of Ni content, the corrosion resistance enhanced first and then dropped. Wu explained that the Ni has relatively small atomic size and its lattice was seriously distorted at high contents [20]. Ye et al. studied the corrosion properties of Al<sub>x</sub>FeCoNiCuCr coatings on 314L stainless steel [28], [38]. The coating had good metallurgical bonding with 314L stainless steel substrate. The relative uniform element distribution within the coatings showed better corrosion resistance than 314 L stainless steel in 0.05M HCl solution, which could be attributed to the additional of Al element.

The process parameters like laser scan speed also influenced the corrosion resistance of HEAs. This can be explained that the higher the scan speed, the less laser energy was absorbed by the HEAs [13]. Therefore, the fast cooling rate made the layer surface smooth and uniform and this helped the corrosion resistance of HEAs.

**Table 3** summaries the electrochemical parameters through the potentiodynamic polarization tests for HEAs in aqueous environments at room temperature. As discussed above, the contents of Al and Ti elements benefit the corrosion resistance of HEAs. The addition of Ni increases the corrosion resistance first and then decreases.

**Table 3 Electrochemical parameters in aqueous environment of HEAs at room temperature**

Alloy	$I_{\text{corr}}^1/\text{Acm}^{-2}$	$E_{\text{corr}}^2/\text{V}_{\text{SCE}}$	Solution	Ref.
FeCoCrAlCuNi <sub>0.5</sub>	$7.84 \times 10^{-7}$	-0.27	3.5 wt.%NaCl	[21]
FeCoCrAlCuNi <sub>1.0</sub>	$3.63 \times 10^{-7}$	-0.25	3.5 wt.%NaCl	[21]
FeCoCrAlCuNi <sub>1.5</sub>	$7.48 \times 10^{-7}$	-0.21	3.5 wt.%NaCl	[21]
Al <sub>2</sub> CrFeCoCuTiNi <sub>0</sub>	$6.8 \times 10^{-5}$	-0.51	3.5 wt.%NaCl	[40]
Al <sub>2</sub> CrFeCoCuTiNi <sub>0.5</sub>	$3.2 \times 10^{-5}$	-0.43	3.5 wt.%NaCl	[40]
Al <sub>2</sub> CrFeCoCuTiNi <sub>1.0</sub>	$1.3 \times 10^{-5}$	-0.22	3.5 wt.%NaCl	[40]
Al <sub>2</sub> CrFeCoCuTiNi <sub>1.5</sub>	$6.4 \times 10^{-5}$	-0.48	3.5 wt.%NaCl	[40]
Al <sub>2</sub> CrFeCoCuTiNi <sub>2.0</sub>	$6.7 \times 10^{-5}$	-0.50	3.5 wt.%NaCl	[40]
Al <sub>1.0</sub> FeCoNiCuCr	$2.92 \times 10^{-5}$	-0.55	0.05M HCl	[28]

Al <sub>1.3</sub> FeCoNiCuCr	4.79×10 <sup>-5</sup>	-0.58	0.05M HCl	[28]
Al <sub>1.5</sub> FeCoNiCuCr	3.14×10 <sup>-5</sup>	-0.92	0.05M HCl	[28]
Al <sub>1.8</sub> FeCoNiCuCr	7.6×10 <sup>-6</sup>	-0.67	0.05M HCl	[28]
Al <sub>2.0</sub> FeCoNiCuCr	3.17×10 <sup>-5</sup>	-0.66	0.05M HCl	[28]
FeCoCrAlNiTi <sub>0.5</sub>	2.0×10 <sup>-7</sup>	-0.2	3.5 wt.%NaCl	[20]
FeCoCrAlNiTi <sub>1.0</sub>	7.3×10 <sup>-8</sup>	-0.23	3.5 wt.%NaCl	[20]
FeCoCrAlNiTi <sub>1.5</sub>	3.2×10 <sup>-7</sup>	-0.175	3.5 wt.%NaCl	[20]
FeCoCrAlNiTi <sub>2.0</sub>	4.7×10 <sup>-7</sup>	-0.19	3.5 wt.%NaCl	[20]
FeCoCrAlCuMo <sub>0.5</sub>	9.57×10 <sup>-7</sup>	-0.21	3.5 wt.%NaCl	[26]
FeCoCrAlCuSi <sub>0.5</sub>	2.37×10 <sup>-7</sup>	-0.26	3.5 wt.%NaCl	[26]
FeCoCrAlCuTi <sub>0.5</sub>	6.01×10 <sup>-7</sup>	-0.23	3.5 wt.%NaCl	[26]

<sup>1</sup>I<sub>corr</sub>: corrosion current density; <sup>2</sup>E<sub>corr</sub>: corrosion potential, V<sub>SCE</sub>: potential versus saturated calomel electrode.

### Conclusions

HEAs are emerging class of metallic materials. The thermodynamic theory and current additive manufacturing methods to fabricate HEAs have been reviewed in this paper. Due to the advantages of additive manufacturing, HEAs possess superior mechanical and corrosion-resistance properties to the conventional alloys. The selection of alloy element and controlling the process parameters are relatively new research topics that hold promise of future HEAs research.

### Acknowledgement

This project was supported by National Science Foundation Grants CMMI-1547042 and CMMI 1625736, and the Intelligent Systems Center, Center for Aerospace Manufacturing Technologies, and Material Research Center at Missouri S&T. Their financial support is greatly appreciated.

### Reference

- [1] B. J. Yeh *et al.*, “Nanostructured High-Entropy Alloys with Multiple Principal Elements : Novel Alloy Design Concepts and Outcomes \*\*,” no. 5, pp. 299–303, 2004.
- [2] J. Yeh, Y. Chen, S. Lin, and S. Chen, “High-Entropy Alloys – A New Era of Exploitation,” vol. 560, pp. 1–9, 2007.
- [3] J. W. Yeh, “Alloy design strategies and future trends in high-entropy alloys,” *Jom*, vol. 65, no. 12, pp. 1759–1771, 2013.
- [4] M. Chuang, M. Tsai, W. Wang, S. Lin, and J. Yeh, “high-entropy alloys,” vol. 59, pp. 6308–6317, 2011.
- [5] Z. Tang *et al.*, “Aluminum alloying effects on lattice types, microstructures, and mechanical behavior of high-entropy alloys systems,” *Jom*, vol. 65, no. 12, pp. 1848–1858, 2013.
- [6] Y. Zhang, X. Yang, and P. K. Liaw, “Alloy design and properties optimization of high-entropy alloys,” *Jom*, vol. 64, no. 7, pp. 830–838, 2012.
- [7] X. Yang and Y. Zhang, “Prediction of high-entropy stabilized solid-solution in multi-

- component alloys,” *Mater. Chem. Phys.*, vol. 132, no. 2–3, pp. 233–238, 2012.
- [8] H. Zhang, Y. Pan, Y. Z. He, J. L. Wu, T. M. Yue, and S. Guo, “Application Prospects and Microstructural Features in Laser-Induced Rapidly Solidified High-Entropy Alloys,” *JOM*, vol. 66, no. 10, pp. 2057–2066, 2014.
- [9] Y. Zhang *et al.*, “Microstructures and properties of high-entropy alloys,” *Prog. Mater. Sci.*, vol. 61, no. September 2013, pp. 1–93, 2014.
- [10] X. Fu, C. A. Schuh, and E. A. Olivetti, “Materials selection considerations for high entropy alloys,” *Scr. Mater.*, 2017.
- [11] C. Haase, F. Tang, M. B. Wilms, A. Weisheit, and B. Hallstedt, “Combining thermodynamic modeling and 3D printing of elemental powder blends for high-throughput investigation of high-entropy alloys – Towards rapid alloy screening and design,” *Mater. Sci. Eng. A*, vol. 688, no. January, pp. 180–189, 2017.
- [12] S. Guo, C. Ng, J. Lu, and C. T. Liu, “Effect of valence electron concentration on stability of fcc or bcc phase in high entropy alloys,” *J. Appl. Phys.*, vol. 109, no. 10, 2011.
- [13] Y. Shi, B. Yang, and P. Liaw, “Corrosion-Resistant High-Entropy Alloys: A Review,” *Metals (Basel)*, vol. 7, no. 2, p. 43, 2017.
- [14] O. N. Senkov, G. B. Wilks, D. B. Miracle, C. P. Chuang, and P. K. Liaw, “Intermetallics Refractory high-entropy alloys,” *Intermetallics*, vol. 18, no. 9, pp. 1758–1765, 2010.
- [15] J. Joseph, T. Jarvis, X. Wu, N. Stanford, P. Hodgson, and D. Mark, “Materials Science & Engineering A Comparative study of the microstructures and mechanical properties of direct laser fabricated and arc-melted Al x CoCrFeNi high entropy alloys,” *Mater. Sci. Eng. A*, vol. 633, pp. 184–193, 2015.
- [16] Y. Brif, M. Thomas, and I. Todd, “The use of high-entropy alloys in additive manufacturing,” *Scr. Mater.*, vol. 99, pp. 93–96, 2015.
- [17] T. Fujieda *et al.*, “First demonstration of promising selective electron beam melting method for utilizing high-entropy alloys as engineering materials,” *Mater. Lett.*, vol. 159, pp. 12–15, 2015.
- [18] W. Gao *et al.*, “Computer-Aided Design The status , challenges , and future of additive manufacturing in engineering,” *Comput. Des.*, vol. 69, pp. 65–89, 2015.
- [19] Z. Cai *et al.*, “Materials Characterization Synthesis and microstructure characterization of Ni-Cr-Co-Ti-V-Al high entropy alloy coating on Ti-6Al-4V substrate by laser surface alloying,” *Mater. Charact.*, vol. 120, pp. 229–233, 2016.
- [20] C. L. Wu, S. Zhang, C. H. Zhang, H. Zhang, and S. Y. Dong, “Phase evolution and cavitation erosion-corrosion behavior of FeCoCrAlNiTi<sub>x</sub> high entropy alloy coatings on 304 stainless steel by laser surface alloying,” *J. Alloys Compd.*, vol. 698, pp. 761–770, Mar. 2017.
- [21] C. L. Wu, S. Zhang, C. H. Zhang, H. Zhang, and S. Y. Dong, “Phase evolution and properties in laser surface alloying of FeCoCrAlCuNi<sub>x</sub> high-entropy alloy on copper substrate,” *Surf. Coatings Technol.*, vol. 315, pp. 368–376, 2017.
- [22] S. Zhang, C. L. Wu, C. H. Zhang, M. Guan, and J. Z. Tan, “Laser surface alloying of FeCoCrAlNi high-entropy alloy on 304 stainless steel to enhance corrosion and cavitation erosion resistance,” *Opt. Laser Technol.*, vol. 84, pp. 23–31, 2016.
- [23] H. Shiratori, T. Fujieda, K. Yamanaka, and Y. Koizumi, “Materials Science & Engineering A Relationship between the microstructure and mechanical properties of an equiatomic AlCoCrFeNi high-entropy alloy fabricated by selective electron beam melting,” *Mater. Sci. Eng. A*, vol. 656, pp. 39–46, 2016.

- [24] D. B. Miracle, J. D. Miller, O. N. Senkov, C. Woodward, M. D. Uchic, and J. Tiley, "Exploration and Development of High Entropy Alloys for Structural Applications," pp. 494–525, 2014.
- [25] S. Katakam, S. S. Joshi, S. Mridha, S. Mukherjee, and N. B. Dahotre, "Laser assisted high entropy alloy coating on aluminum: Microstructural evolution," *J. Appl. Phys.*, vol. 116, no. 10, pp. 0–6, 2014.
- [26] C. L. Wu, S. Zhang, C. H. Zhang, J. Chen, and S. Y. Dong, "Phase evolution characteristics and corrosion behavior of FeCoCrAlCu-X0.5 coatings on cp Cu by laser high-entropy alloying," *Opt. Laser Technol.*, vol. 94, pp. 68–71, 2017.
- [27] H. Rakshit, J. W. Newkirk, and F. F. Liou, "Effect of Al / Ni ratio , heat treatment on phase transformations and microstructure of Al x FeCoCrNi 2 Å x ( x = 0 . 3 , 1 ) high entropy alloys," *Mater. Des.*, vol. 81, pp. 113–121, 2015.
- [28] X. Ye, M. Ma, Y. Cao, W. Liu, X. Ye, and Y. Gu, "The property research on high-entropy alloy AlxFeCoNiCuCr coating by laser cladding," *Phys. Procedia*, vol. 12, no. PART 1, pp. 303–312, 2011.
- [29] I. Kunc, M. Polanski, K. Karczewski, T. Plocinski, and K. J. Kurzydowski, "Microstructural characterisation of high-entropy alloy AlCoCrFeNi fabricated by laser engineered net shaping," *J. Alloys Compd.*, vol. 648, pp. 751–758, 2015.
- [30] T. Amine, J. W. Newkirk, and F. Liou, "Case Studies in Thermal Engineering An investigation of the effect of direct metal deposition parameters on the characteristics of the deposited layers," *Case Stud. Therm. Eng.*, vol. 3, pp. 21–34, 2014.
- [31] F. Authors, "Binding mechanisms in selective laser sintering and selective laser melting," 2005.
- [32] S. Bremen and W. Meiners, "Selective Laser Melting A manufacturing technology for the future ?," pp. 33–38, 2012.
- [33] T. Fujieda, H. Shiratori, K. Kuwabara, M. Hirota, and T. Kato, "CoCrFeNiTi-based high-entropy alloy with superior tensile strength and corrosion resistance achieved by a combination of additive manufacturing using selective electron beam melting and solution treatment," *Mater. Lett.*, vol. 189, no. November 2016, pp. 148–151, 2017.
- [34] N. Read, W. Wang, K. Essa, and M. M. Attallah, "Selective laser melting of AlSi10Mg alloy : Process optimisation and mechanical properties development," *Mater. Des.*, vol. 65, pp. 417–424, 2015.
- [35] J. Joseph, N. Stanford, P. Hodgson, and D. M. Fabijanic, "Tension/compression asymmetry in additive manufactured face centered cubic high entropy alloy," *Scr. Mater.*, vol. 129, pp. 30–34, 2017.
- [36] V. Ocelak, N. Janssen, S. N. Smith, and J. T. M. De Hosson, "Additive Manufacturing of High-Entropy Alloys by Laser Processing," *JOM*, vol. 68, no. 7, pp. 1810–1818, 2016.
- [37] E. J. Pickering and N. G. Jones, "High-entropy alloys: a critical assessment of their founding principles and future prospects," *Int. Mater. Rev.*, vol. 61, no. 3, pp. 183–202, 2016.
- [38] X. Ye *et al.*, "Synthesis and Characterization of High-Entropy Alloy FeCoNiCuCr by Laser Cladding," *Adv. Mater. Sci. Eng.*, vol. 2011, pp. 1–7, 2011.
- [39] S. Zhang, C. L. Wu, J. Z. Yi, and C. H. Zhang, "Synthesis and characterization of FeCoCrAlCu high-entropy alloy coating by laser surface alloying," *Surf. Coatings Technol.*, vol. 262, pp. 64–69, 2015.
- [40] X. Qiu and C. Liu, "Microstructure and properties of Al 2 CrFeCoCuTiNi x high-entropy

- alloys prepared by laser cladding,” *J. Alloys Compd.*, vol. 553, pp. 216–220, 2013.
- [41] M. Zhang, X. Zhou, X. Yu, and J. Li, “Synthesis and characterization of refractory TiZrNbWMo high-entropy alloy coating by laser cladding,” *Surf. Coatings Technol.*, vol. 311, pp. 321–329, 2017.
- [42] X. Wang, X. Gong, and K. Chou, “Review on Powder-Bed Laser Additive Manufacturing of Inconel 718 Parts,” pp. 1–9, 2017.
- [43] D. Zhang, W. Niu, X. Cao, and Z. Liu, “Materials Science & Engineering A Effect of standard heat treatment on the microstructure and mechanical properties of selective laser melting manufactured Inconel,” vol. 644, pp. 32–40, 2015.
- [44] E. Akca and A. Gursel, “A Review on Superalloys and IN718 Nickel-Based INCONEL Superalloy,” vol. 3, no. 1, 2015.
- [45] R. Wang, K. Zhang, C. Davies, and X. Wu, “Evolution of microstructure , mechanical and corrosion properties of AlCoCrFeNi high-entropy alloy prepared by direct laser fabrication,” *J. Alloys Compd.*, vol. 694, pp. 971–981, 2017.
- [46] Y. Shon, S. S. Joshi, S. Katakam, R. Shanker, and N. B. Dahotre, “Laser additive synthesis of high entropy alloy coating on aluminum : Corrosion behavior,” *Mater. Lett.*, vol. 142, pp. 122–125, 2015.
- [47] K. K. Alaneme, M. O. Bodunrin, and S. R. Oke, “Processing, alloy composition and phase transition effect on the mechanical and corrosion properties of high entropy alloys: A review,” *J. Mater. Res. Technol.*, vol. 5, no. 4, pp. 384–393, 2016.
- [48] T. M. Butler and M. L. Weaver, “Investigation of the phase stabilities in AlNiCoCrFe high entropy alloys,” *J. Alloys Compd.*, vol. 691, pp. 119–129, 2017.